In vitro birefringence imaging with spectral domain polarization-sensitive optical coherence tomography

Qiang Gong (龚 强)[1,2], Chuanmao Fan (范传茂)[1,2], Fan Zhang (张 帆)[1,2], and Jianquan Yao (姚建铨)[1,2]

[1]*Key Laboratory of Optoelectric Information Science and Technology, Ministry of Education, Tianjin University, Tianjin 300072*

[2]*Institute of Laser and Optoelectronics, College of Precision Instrument and Optoelectronics Engineering, Tianjin University, Tianjin 300072*

Received June 18, 2008

Spectral domain polarization-sensitive optical coherence tomography (SDPS-OCT) is a depth-resolved polarization-sensitive interferometry which integrates polarization optics into spectral domain optical coherence tomography (SD-OCT). This configuration can obtain birefringence information of samples and improve the imaging speed. In this paper, horizontally polarized light is used to replace natural light of the source. Then, right-rotated circularly polarized light is the incident sample light. To obtain two orthogonal components of the polarized interferogram, the reflected light of the reference arm is set to be 45° linearly polarized light. These two components are acquired by two spectrometers synchronously. The system was employed to achieve 12.8-μm axial resolution and 4.36-μm transverse resolution. We have imaged *in vitro* chicken tendon and muscle tissues with these system.

OCIS codes: 170.4500, 110.4500, 260.1440, 260.5430.

doi: 10.3788/COL20080612.0905.

Optical coherence tomography (OCT) is a noninvasive, non-destructive technique with high scanning speed and resolution developed by Huang *et al.* in 1991[1]. The configuration is based on Michelson interference theory. In an OCT system, the light beam focused on the sample is reflected from different layers, and then interferes with the light reflected from the reference arm. The interference signal includes the structure information of the sample. However, the initial OCT system is based on temporal domain, and the depth information should be obtained by point-to-point movement of the reference arm. Therefore, the scanning speed it greatly limited. After several years, a novel OCT system named as spectral radar was developed by Fercher *et al.*[2]. In this system, depth information was directly obtained by Fourier transformation of interference interferogram so that scanning in depth is deleted. Now, it is named as spectral domain OCT (SD-OCT)[3,4]. In 1998, Häusler *et al.* developed a fiber-based SD-OCT system and imaged human skin tissues with this system[5]. Though SD-OCT gets an improved scanning speed, it obtains depth signal by using amplitude information of backscattering reflectance from samples. Therefore, it still belongs to structure imaging. Nowadays, researchers increasingly found that collagen commonly existed in biological tissues[6−11]. Anisotropy property of collagen causes birefringence, which can lead to changes of phase delay and fast axis angle of samples when polarized light is focused on it. Therefore, polarization-sensitive OCT (PS-OCT) is gradually developed as a novel OCT imaging method[12−17]. In PS-OCT, special polarized light is used to detect the sample, and the interference signal of backscattering light of the sample includes special anisotropy information. In this paper, we apply polarized optics in SD-OCT system, and analyze polarized imaging principles in spectral domain. At the same time, we deduce the additional phase delay and the fast axis angle of the sample besides depth structure image. *In vitro* biological tissues are used as sample to demonstrate the feasibility of the system.

As we all know, in SD-OCT, backscattering light of samples will interfere with the reflected light of reference arm within coherence length. The length information consists of elementary waves reflected from different depth z which are corresponding to the scattering amplitude from different depth $a(z)$. After interference, the interfering signal $I(K)$ can be expressed[18]

$$I(K) = S(K)\{a_{\rm R}^2 + 2a_{\rm R}\int_0^\infty a(z)\exp(-i\cdot 2Knz)\mathrm{d}z + \int_0^\infty\int_0^\infty a(z)a(z')\exp[i\cdot 2K(nz-nz')]\mathrm{d}z\mathrm{d}z'\}, \quad (1)$$

where $S(K)$ is the spectral density of the source; $a_{\rm R}$ is the reference arm amplitude; $a(z)$ is the backscattering amplitude of the sample, when $z < z_0$, $a(z) = 0$; n is the refractive index of the sample; K is wave number. In Eq. (1), the three terms in the brackets represent different meanings. The first one is the auto-correlation density of the reference arm; the second one includes depth amplitude information, which is a superposition of different frequency cosine components; the last one is the auto-correlation density of the sample arm from correlation of backscattering of different depth. The source signal and interference signal are shown in Fig. 1.

After fast Fourier transformation (FFT) to Eq. (1), it is deduced that

$$H(z) = \mathrm{FOU}^{-1}\{I(K)\} = \mathrm{FOU}^{-1}\{S(K)\}\otimes\{a_{\rm R}^2\delta(z) + a_{\rm R}[a(z)+a^*(-z)] + AC(I_{\rm au}(K))\} = A\otimes(B+C+D), \quad (2)$$

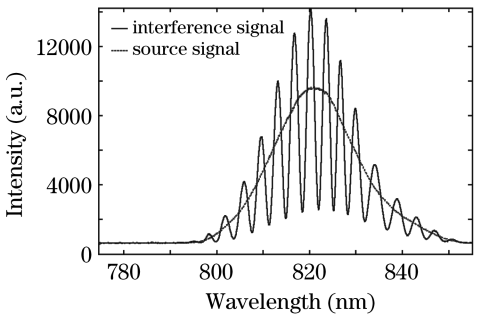

Fig. 1. Interference and source signals.

where AC is the autocorrelation term of scattering elementary waves, and

$$I_{\mathrm{au}}(K) = \int_0^\infty \int_0^\infty a(z)a(z')\exp\left[i\cdot 2K\left(nz-nz'\right)\right]\mathrm{d}z\mathrm{d}z', \quad (3)$$

$\otimes$ is the convolution symbol. A is the FFT result of light source. In Eq. (2), $A\otimes B$ is the FFT term of light source spectrum when $z=0$, which is named as zero phase noise term; $A\otimes C$ is the depth information of the sample $a(z)$ after FFT, including virtual image information; $A\otimes D$ is the auto-correlation term, which represents the correlation between different scattering elementary waves.

For SD-OCT, the above description can obtain depth information of the detected sample, which is generally named as structure imaging because all depth information is from the backscattering light of the sample. However, biological tissues provides more than structure information. Birefringence is another popular phenomenon in biological organisms, which is one of the most important parameters in biological tissue detection. This phenomenon is caused by the component of collagen, whose most notable feature is birefringence property and three-dimensional spiral structure[11]. Polarization of material has close relationship with its birefringence. Therefore, we can utilize the polarization change of light to obtain the birefringence of tissues. Here, we apply polarization optics into SD-OCT system. Its expression is based on Jones vectors and matrix. In Jones matrix, a retarder can be expressed as[17]

$$J(\delta,\varepsilon) = \begin{bmatrix} \cos^2\varepsilon + \sin^2\varepsilon\cdot\exp(-i\delta) & \cos\varepsilon\cdot\sin\varepsilon\cdot(1-\exp(-i\delta)) \\ \cos\varepsilon\cdot\sin\varepsilon\cdot(1-\exp(-i\delta)) & \cos^2\varepsilon\cdot\exp(-i\delta)+\sin^2\varepsilon \end{bmatrix}, \quad (4)$$

where ε is the angle between the fast axis and the horizontal direction, δ is the delayed phase of the retarder. If a polarized light E_{i} propagated through series of polarized components J_1, J_2, $\cdots$, J_{n-1}, then the polarization of the output light E_{o} is[19]

$$E_{\mathrm{o}} = J_{n-1}\cdot\ \cdots\ \cdot J_2\cdot J_1\cdot E_{\mathrm{i}}. \quad (5)$$

According to the above expressions, we designed a spectral domain PS-OCT (SDPS-OCT) system to obtain the birefringence image of the sample, as shown in Fig. 2. In this system, we used the right-rotated circularly polarized light as the sample arm, and 45° linearly polarized light as the reference arm. The special birefringence information is included into the output backscattering sample beam, which interferes with the reference beam. Jones matrix of the sample $M_{\mathrm{sample}}(z,\Delta n,\alpha)$ is assumed as the continued multiplication of averaged phase delay, rotated matrix, and linear retarder with a horizontal fast axis. According to Eqs. (4) and (5), the Jones matrix of the sample is

$$M_{\mathrm{sample}}(z,\Delta n,\alpha) = \exp(-iKz\bar{n}) \begin{pmatrix} \cos^2\alpha+\sin^2\alpha\cdot\exp(-iKz\Delta n/2) & \cos\alpha\cdot\sin\alpha\cdot(1-\exp(-iKz\Delta n/2)) \\ \cos\alpha\cdot\sin\alpha\cdot(1-\exp(-iKz\Delta n/2)) & \cos^2\alpha\cdot\exp(-iKz\Delta n/2)+\sin^2\alpha \end{pmatrix}, \quad (6)$$

where $Kz\bar{n}$ is the average phase delay of the sample, $\bar{n}$ is the average refractive index, $\bar{n}=(n_{\mathrm{s}}+n_{\mathrm{f}})/2$ with n_{s} and n_{f} representing the indices along slow and fast axes, $\Delta n = n_{\mathrm{s}}-n_{\mathrm{f}}$ is the difference between the slow and fast axes of the sample, α is the angle of the fast axis, the phase delay that the light passes through the sample just once is $\delta = Kz\Delta n$. Therefore, the Jones vector of the backscattering light of the sample is the product between the polarized sample light and the detected optical component. In this process, the sample light passes through retarder 1 and detects the sample twice, so that the Jones vector of backscattering light E_{s} at point a in Fig. 2 is

$$E_{\mathrm{s}}(z+z_{\mathrm{s}}) = \begin{pmatrix} E_{\mathrm{sh}} \\ E_{\mathrm{sv}} \end{pmatrix} = \frac{1}{2}J_{d1}M_{\mathrm{sample}}(z,\Delta n,\alpha) \cdot\sqrt{R(z)}M_{\mathrm{sample}}(z,\Delta n,\alpha)J_{d1}E_{\mathrm{si}}, \quad (7)$$

where $R(z)$ is the reflectance of backscattering light in depth z, z_{s} is the distance from the beam splitter (BS) to the surface of the sample, E_{sh} and E_{sv} are the horizontal and vertical parts of the backscattering light. The retarders 1 and 2 are both 1/4 wave plates, so here we use J_{d1} and J_{d2} to represent their Jones matrices.

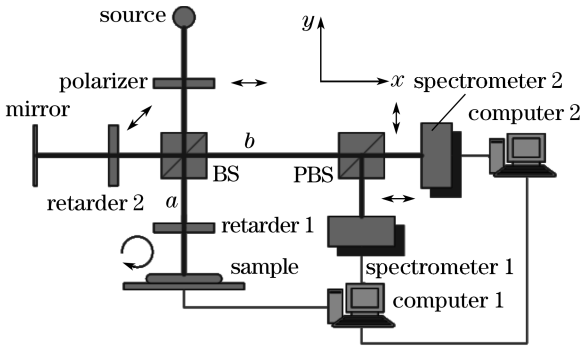

Fig. 2. Configuration of SDPS-OCT system.

The source light through polarizer is horizontally linearly polarized light. After the BS, the incident light beams in the sample and reference arms are

$$E_{\mathrm{si}} = E_{\mathrm{ri}} = \frac{E(K,z)}{2}\begin{bmatrix} 1 \\ 0 \end{bmatrix}. \tag{8}$$

After reflection, the light of the reference arm passes through a 22.5° 1/4 wave plate, so it can be expressed as

$$E_{\mathrm{r}}(K,z_{\mathrm{r}}) = \begin{bmatrix} E_{\mathrm{rh}} \\ E_{\mathrm{rv}} \end{bmatrix} = \frac{1}{2}J_{d2}J_{d2}E_{\mathrm{ri}} = \frac{1}{2}E(K,2z_{\mathrm{r}})\begin{bmatrix} 1 \\ 1 \end{bmatrix}. \tag{9}$$

For the sample arm, according to Eq. (7) and (8) and Wiener-Khintchine theorom, the Jones vetor of the backscattering light of the sample has the following relationship:

$$E_{\mathrm{s}}(z+z_{\mathrm{s}}) \propto \sqrt{R(z)}E(K,z_{\mathrm{s}}+z_{\bar{n}})\begin{bmatrix} \exp(2i\alpha)\sin(Kz\Delta n) \\ \cos(Kz\Delta n) \end{bmatrix}. \tag{10}$$

After interference between the sample and reference arms, the horizontal and vertical polarized components can be obtained by the polarization beam splitter (PBS)

$$E_{\mathrm{inf}} = \begin{bmatrix} E_{\mathrm{inf\_h}} \\ E_{\mathrm{inf\_v}} \end{bmatrix} = \begin{bmatrix} S(K)\left\langle a_{\mathrm{R}}\exp(i\cdot 2Kr) + \int_0^{\infty}\sqrt{R(z)}\sin(Kz\Delta n)\exp\{i\cdot[2K(r+n(z)z)+2\alpha]\}\,\mathrm{d}z\right\rangle \\ S(K)\left\langle a_{\mathrm{R}}\exp(i\cdot 2Kr) + \int_0^{\infty}\sqrt{R(z)}\cos(Kz\Delta n)\exp\{i\cdot 2K(r+n(z)z)\}\,\mathrm{d}z\right\rangle \end{bmatrix}, \tag{11}$$

where $\sqrt{R(z)}\sin(Kz\Delta n)$ and $\sqrt{R(z)}\cos(Kz\Delta n)$ represent the orthogonal components of the interference signal, which also give the backscattering amplitude of the light. After FFT transformation, we can get

$$\begin{aligned} H_{\mathrm{inf}}(z) &= \begin{bmatrix} H_{\mathrm{inf\_h}} \\ H_{\mathrm{inf\_v}} \end{bmatrix} \\ &= \mathrm{FOU}^{-1}\{S(K)\} \otimes \begin{bmatrix} a_{\mathrm{R}}^2\delta(z) + a_{\mathrm{R}}\exp(-i\cdot 2\alpha)\left[\sqrt{R(z)}\sin(Kz\Delta n) + \left(\sqrt{R(-z)}\sin(K-z\Delta n)\right)^*\right] + AC(I_{\mathrm{au}}(K)) \\ a_{\mathrm{R}}^2\delta(z) + a_{\mathrm{R}}\left[\sqrt{R(z)}\cos(Kz\Delta n) + \left(\sqrt{R(-z)}\cos(K-z\Delta n)\right)^*\right] + AC(I_{\mathrm{au}}(K)) \end{bmatrix}. \end{aligned} \tag{12}$$

In Eq. (12), the vertical part has an additional 2α phase delay to the horizontal part, which indicates the fast axis information. Then, the backscattering reflectance $R(z)$ and phase delay $\delta(z)$[17] is

$$R(z) = H_{\mathrm{inf\_h}}^2(z) + H_{\mathrm{inf\_v}}^2(z), \tag{13a}$$

$$\delta(z) = \arctan\left[H_{\mathrm{inf\_h}}/H_{\mathrm{inf\_v}}\right]. \tag{13b}$$

The direction of the fast axis is the difference between these two orthogonal parts,

$$\alpha = \frac{\pi - (\Phi_{\mathrm{h}} - \Phi_{\mathrm{v}})}{2}, \tag{14}$$

where Φ_{h} and Φ_{v} are the phases of the two orthogonal parts.

All the description above is the process of obtaining the birefringence information of the sample in SDPS-OCT system. Special polarized incident light is used as sample and reference beams, and after interference, the orthogonal polarized components are obtained to compute the backscattering reflectance, the phase delay, and the fast axis direction of the sample. The latter two terms are used to describe the birefringence information.

To eliminate the zero phase, autocorrelation and virtual image terms of the two orthogonal components in Eq. (12), we apply five-phase shifting method in signal processing of the system. The mirror of the reference arm is positioned on a piezoelectric transducer (PZT) device, which can move with a $\pi/2$ step. So each frame includes five data groups actually, H_1, H_2, H_3, H_4, H_5. The phase of interferogram is

$$\Phi(K) = \frac{2(H_2 - H_4)}{H_1 - 2H_3 + H_5}. \tag{15}$$

To demonstrate the feasibility of our SDPS-OCT system, we imaged two *in vitro* biological tissues with our laboratory system. Because the transverse and depth resolution in OCT is independent, we can calculate them with the system parameters[18]. In the constructed system, a superluminescent diode (SLD) was used as illuminating source. Its center wavelength was 822.5 nm with the full-width at half-maximum (FWHM) of 23.5 nm. Therefore, we can calculate the depth resolution of the system to be 12.8 μm. A micro-motion device was used for transverse scanning, and its transverse resolution was 0.125 μm. The numerical aperture (NA) of the focusing lens of the sample arm was 0.1. So we can obtain the transverse resolution of the SDPS-OCT system is 4.36 μm. The configuration of the system has been shown in Fig. 2.

Firstly, *in vitro* chicken tendon was used as the detected sample. The tendon consists of coarse-shape collagen

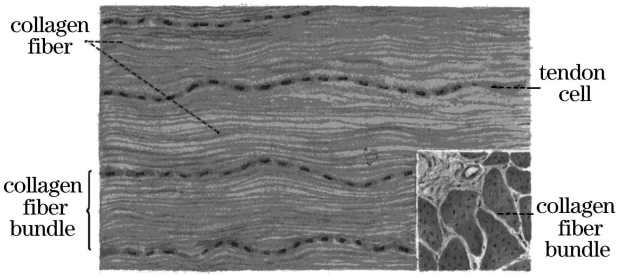

Fig. 3. Anatomical image of tendon.

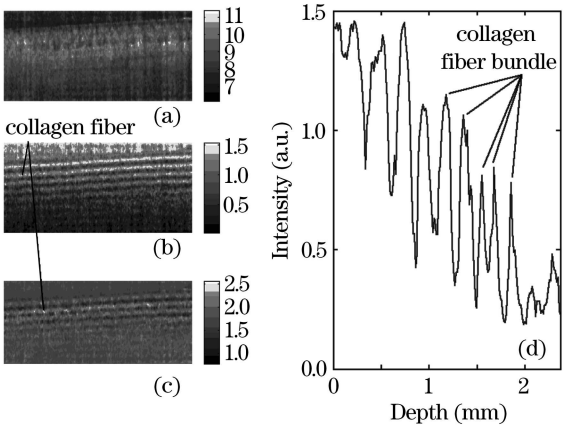

Fig. 4. *In vitro* chicken tendon images by SDPS-OCT system. (a) Backscattering reflectance image; (b) phase delay image; (c) fast axis image; (d) phase delay image for one frame.

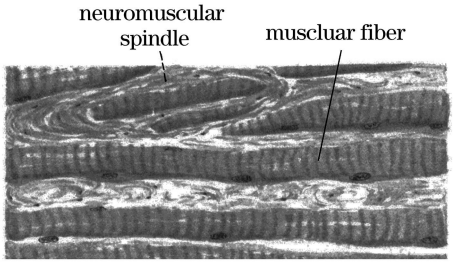

Fig. 5. Anatomical image of muscle.

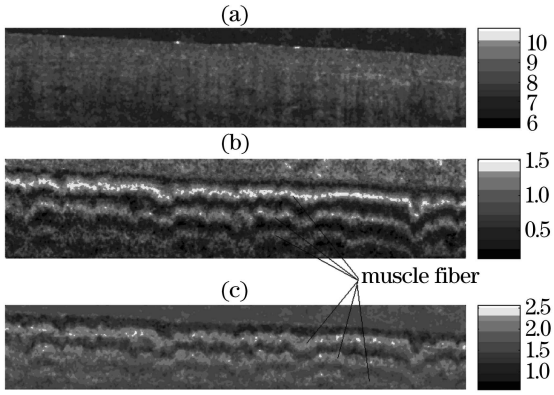

Fig. 6. Birefringence images of *in vitro* chicken muscle. (a) Backscattering reflectance image; (b) phase delay image; (c) fast axis image.

fiber bundles with regular arrangement, as shown in Fig. 3. We collected the horizontally and vertically polarized components, and then by Eqs. (13) and (14), we can calculate the backscattering reflectance, the phase delay, and the fast axis angle of tendon. The images are shown in Fig. 4, each image is 1366×1000 pixels in size, and the imaging area is $x \times z = 4.36 \times 2.37$ (mm).

In Figs. 4(b) and (c), we can clearly observe that because of the periodic arrangement of collagen fiber bundles in tendon, the images present regular changes. In the tendon, the birefringence of collagen fiber bundles leads to the periodic change in depth, and this change is reflected in the phase delay of backscattering light. The bright fringes in Fig. 4 represent the collagen fibers. The image of the fast axis includes the anisotropy property of tendon.

To validate the SDPS-OCT system further, we also imaged *in vitro* chicken muscle as another demonstration. The advantage of selecting muscle is that the tissue exists more apparent periodic layers of collagen, and the muscle fiber bundles have a large diameter. In our experiment, the chicken skeletal muscle sample used in this study was obtained immediately after slaughtering. During the experiment, we cut one piece of sample with the dimensions of $3 \times 3 \times 1$ (cm). The skeletal muscle was mounted in a holder with fibrous tissue approximately parallel with the B scanning mode, and then fixed so that it did not move during the imaging. The shape of the detected skeletal muscle is a long column along muscle fibers, as shown in Fig. 5.

Figure 6 shows the birefringence images of *in vitro* chicken muscle detected by our SDPS-OCT system. The images are 1366×1000 pixels in size, and the imaging area is also $x \times z = 4.36 \times 2.37$ (mm). Figure 6(a) is the backscattering reflectance image. We can observe that no layered structure is present. However, in Figs. 6(b) and (c), muscle fibers are clearly shown, and at the same time, we can find that all the fibers exhibit a periodic change. Such a structure is consistent with the anatomical image in Fig. 5. Skeletal muscle fiber consists of bundles of muscle fibers with the diameter of ~ 50 μm. Muscle fibers are composed of bundles of myofibrils which are about 1 μm in diameter. The birefringence of muscle fibers causes the phase delay of polarized backscattering light to change with depth. Compared with the tendon images, muscle fiber images have a clearer and larger diameter, and its arrangement is as regular as tendon. In the two experiments, birefringence causes the horizontally and vertically polarized interferograms with phase difference to change with depth. Moreover, anisotropy of detected tissue change fast axis of sample. Therefore, we also can acquire the change of fast axis with depth. Fast axis image is also corresponding to tissues structure and reflects arrangement of tendon and muscle fiber.

In summary, a SDPS-OCT system has been developed in this paper. With this system, the additional birefringence information can be obtained by acquiring the horizontally and vertically polarized interferograms. Because those two orthogonal components change with the depth structure of collagen fiber bundles, the phase delay and fast axis angle of the sample change with the depth of sample. After acquiring two orthogonal components, we applied five-phase shifting method to reconstruct the depth images. To validate our system, we used it to image two *in vitro* biological tissues. Not only the structure or backscattering reflectance image, but also the periodic layered structure of collagen fiber bundles in

tissues could be obtained. This provided additional birefringence information of tissues from anisotropy property of samples. However, in the myofibrils, a single sarcomere extends between two "z discs", the I-bands (bright bands) and A-bands (dark bands) appear where the connection between sarcomere and 'z disc' repeats periodically along the myofibrils. The muscle fibers account for the presence of the birefringence in the skeletal muscle because of the imaging resolution limit of the SDPS-OCT system which images the polarization properties in a macro-scale. Additionally, in our experiment, the theory of PS-OCT is based on the work of Hee *et al.*[20]. The detected sample is assumed to be of pure birefringence, and the information processing methods come from these assumptions. But actually, turbid samples such as tissues are all depolarization ones. The limitation of the presented detection scheme is the inability to determine fully the backscattered light polarization state. The complete characterization of the polarization states is presented by Stokes parameters which permit the calculation of the degree of the polarization. This is our future work.

Q. Gong's e-mail address is gongqiang@aoe.ac.cn.

References

1. D. Huang, E. A. Swanson, C. P. Lin, J. S. Schuman, W. G. Stinson, W. Chang, M. R. Hee, T. Flotte, K. Gregory, C. A. Puliafito, and J. G. Fujimoto, Science **254,** 1178 (1991).
2. A. F. Fercher, C. K. Hitzenberger, G. Kamp, and S. Y. El-Zaiat, Opt. Commun. **117,** 43 (1995).
3. P. Bu, X. Wang, and O. Sasaki, Acta Opt. Sin. (in Chinese) **27,** 1470 (2007).
4. Y. Chen, Z. Ding, and J. Meng, Chinese J. Lasers (in Chinese) **34,** 825 (2007).
5. G. Häusler and M. W. Lindner, J. Biomed. Opt. **3,** 21 (1998).
6. H. M. Jones, R. J. Baskin, and Y. Yeh, Biophys. J. **60,** 1217 (1991).
7. P. Whittaker and P. B. Canham, Matrix **11,** 56 (1991).
8. A. Boyde, P. Bianco, M. P. Barbos, and A. Ascenzi, Metab. Bone Dis. Relat. Res. **5,** 299 (1984).
9. Y. E. Yarker, R. M. Aspden, and D. W. L. Hukins, Connect. Tissue Res. **11,** 207 (1983).
10. R. Ortmann, Anat. Embryol. **148,** 109 (1975).
11. V. Sankaran and J. T. Walsh, Jr., Photochem. Photobiol. **68,** 846 (1998).
12. V. J. lafelice and W. S. Bickel, Appl. Opt. **26,** 2410 (1987).
13. J. F. de Boer, T. E. Milner, M. J. C. van Gemert, and J. S. Nelson, Opt. Lett. **22,** 934 (1997).
14. J. F. de Boer, S. M. Srinivas, A. Malekafzali, Z. Chen, and J. S. Nelson, Opt. Express **6,** 212 (1998).
15. M. J. Everett, K. Schoenenberger, B. W. Colston, Jr., and L. B. Da Silva, Opt. Lett. **23,** 228 (1998).
16. K. Schoenenberger, B. W. Colston, Jr., D. J. Maitland, L. B. Da Silva, and M. J. Everett, Appl. Opt. **37,** 6026 (1998).
17. C. K. Hitzenberger, E. Götzinger, M. Sticker, M. Pircher, and A. F. Fercher, Opt. Express **9,** 780 (2001).
18. M. W. Lindner, P. Andretzky, F. Kiesewetter, and G. Häusler, in *Handbook of Optical Coherence Tomography* B. E. Bouma and G. J. Tearney, (eds.) (Marcel Dekker, New York, 2002) pp.335 − 357.
19. Y. Lu and B. Lü, *Matrix Optics* (in Chinse) (Dalian University of Technology Press, Dalian, 1989) p.322.
20. M. R. Hee, D. Huang, E. A. Swanson, and J. G. Fujimoto, J. Opt. Soc. Am. B **9,** 903 (1992).